Bidirectional Single-Fiber Filterless Optical Networks: modeling and experimental assessment

DIMITRIS UZUNIDIS[1*], MARCO PRESI[2], ANDREA SGAMBELLURI[2], FRANCESCO PAOLUCCI[2,3], ALEXANDROS STAVDAS[4], FILIPPO CUGINI[3]

[1]*OpenLightComm Ltd., London, UK*
[2]*Scuola Superiore Sant'Anna, Pisa, Italy*
[3]*CNIT, Pisa, Italy*
[4]*University of Peloponnese, Tripolis, Greece*
**Corresponding author: duzunidis@hotmail.com*

Received 1 October 2020; revised 1 December, 2020; accepted XX Month XXXX; posted XX Month XXXX (Doc. ID XXXXX); published XX Month XXXX

This paper proposes, designs and validates filterless metro network employing bidirectional transmission over a single fiber. Transmission impairments, dominated by crosstalk, are specifically estimated leveraging on novel close-form expressions to determine optical reach, launch power, and number of supported cascaded nodes. Results show that extremely good transmission performance can be achieved, further improved when misalignment in spectrum allocation is configured among the two counter-propagating directions. This confirms that filterless metro networks employing bidirectional transmission over a single fiber represent an extremely attractive solution, particularly in case of scarce fiber availability and when regulatory aspects impose a rent for any occupied fiber infrastructure. © 2020 Optical Society of America

http://dx.doi.org/10.1364/JOCN.99.099999

1. INTRODUCTION

The history of filterless optical networks already spans a period of twenty years [1, 2]. During this period, filterless network topologies were considered in a number of networking studies and implementations. In [1],[3] a filterless network was proposed in the framework of the European project IST –DAVID for the introduction of Optical Packet Switching (OPS) in metro networks. In this context, there were benchmarking studies which addressed the physical layer performance of this architecture [4], and the potential capital and operational expenditure (CapEx/OpEx) gains [5] it was offering. Extending this initial concept and methodology, the applicability of filterless solutions to the construction of low-cost Core network deployments has been considered in [6-20], confirming the importance of this optical networking paradigm. More recently, the interest for filterless networking solutions has resurfaced to support 5G metro/x-haul scenarios [20-25]. In addition, the current interest in Metro has moved from non-return-to-zero (NRZ) systems as in [1-5] to coherent detection and Pulse Amplitude Modulation (PAM) systems.

A common feature for all filterless solutions is that they exploit an optical transport infrastructure that is built by means of splitters/couplers and amplifiers. In these networks, wavelength channels are not erased from the transport network, after they are dropped at a given node, so there is no need for expensive Reconfigurable Optical Add/Drop Multiplexers (ROADM) and Wavelength Selective Switches (WSS). As such, the term 'filterless' refers to the absence of ROADMs or WSSs in the 'through' part of the transit nodes in the transport network. Still though, (de)multiplexing devices might be in use in filterless networks as their absence could lead to performance degradation [15].

Networking based on filterless configurations is attractive as it offers important cost savings and operational simplifications while it avoids potentially harmful effects, like filter narrowing due to filter cascade. A disadvantage of filterless solutions is that a wavelength channel cannot be erased, therefore it may circulate within a transport network 'indefinitely'. To prevent this, a particular wavelength channel is used only in non-overlapping paths. As a result, filterless solutions either apply only to specific network topologies e.g. a horseshoe/bus as

shown in Fig. 1(a) or wavelength-reuse is limited such that most of the available optical spectrum is underutilized/wasted. Research efforts are concentrated to overcome these limitations and some approaches are discussed in section 2.

In this paper, we propose, study and validate a filterless Metro network exploiting bidirectional transmission over a single fiber. This solution would be of great interest in the case of scarce fiber availability as well as in scenarios where regulatory aspects impose Service Providers to pay a rent to a government body/agency for any occupied fiber infrastructure (e.g. in UK). In section 3, the principle of operation for a bidirectional transmission over a single fiber in Metro is elaborated and the corresponding node architecture is detailed. In section 4, as a proof-of-concept, the performance degradation due to Rayleigh scattering is experimentally validated with two counter-propagating channels. In sections 5 and 6, a methodology to study the physical layer performance of a multi-channel bidirectional transmission system is presented and its scalability is deduced. This article is the invited expanded version of the conference paper [26]. However, the content in Sections 5 and 6 was not included in [26] and it is here presented for the first time.

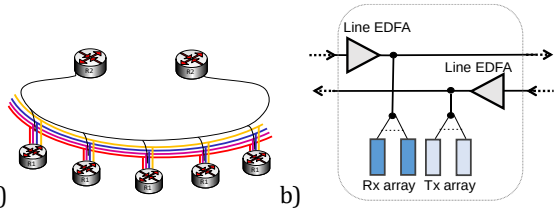

Fig. 1: (a) Horseshoe optical network; (b) A generic filterless node exploiting two unidirectional fibers.

2. FILTERLESS NETWORKS INTO PERSPECTIVE

As it was stated in the previous section, all filterless networks are facing spectrum utilization and topology scalability limitations. The means and the methods employed to overcome these challenges are closely linked to the type of network in mind and its mode of operation. Generally speaking, efforts have been made at both the architectural and system level.

Regarding the different architectural approaches, the main differentiating factor is whether network nodes are considered to belong to the same, single, Core network or a hierarchical solution spanning Metro and Core segments is sought. In the former case, a Routing and Wavelength Assignment (RWA) algorithm was proposed to design a loop-free operation in mesh topologies avoiding light recirculation. Moreover, the work in [7] benchmarks the overall cost of filterless against WSS-based mesh networks and confirms the corresponding findings in [5] that show a remarkable advantage in favor of filterless solutions.

A different approach is followed by researchers focusing in Metro networks. In [3], [21] and [26], as well as in this work, the main interest is to propose and validate architectural solutions that enhance both spectrum utilization and performance within a Metro network segment. Moreover, the works in Metro are further distinguished in the way the optical spectrum is explored: in [21] and [26] Constant-Bit-Rate (CBR) transmission is considered while in [3] and [27] Burst-Mode (BM) systems under a slotted format are employed. In any case, the work in [3], [21], [26] and [27] designate that a bus or a horseshoe-topology exploiting either a unidirectional or a bidirectional transmission are of great interest and, in fact, they could serve as network building blocks upon which more complex (semi) filterless networks can be constructed. For example, node clustering can be explored to allow wavelength re-use and in this case to limit spectral waste. The extension of a filterless horseshoe Metro to construct filterless or semi-filterless networks of larger dimensions has been primarily studied for networks under a slotted operation using BM systems. In [28-30], dynamic or static node clustering is considered while a partially meshed network node topology for the intra-cluster network is decomposed to a number of partially overlapping horseshoe or bus networks. For those networks, bidirectional transmission is of great interest to enhance agility.

Apart from the innovations at an architectural level, several solutions at system level have been proposed to improve the spectrum usage of filterless networks and/or their performance. In [13], the supply of optical power to the receivers in filterless networks (i.e., received power overload) is proposed. In [20], an interesting semi-filterless approach is introduced leveraging on wavelength blockers. In [22], multi-band resources are introduced, providing a differentiated spectrum assignment according to the expected per-band impairment. In [23, 24], rates at 400G and multi-band filterless transmission are considered. In [14], [24] control-plane solutions tailored to filterless networks are implemented in the context of an optical "white box". Finally, in [10] a pilot filterless network implementation is reported with a system employing 100 Gb/s channels spaced by 50GHz that are transmitted over a horseshoe topology. The transmission impairments here are accounted by considering a distance of the horseshoe of around 600 km, including up to N=8 add/drop sites.

On the other hand, bidirectional transmission over a single fiber has been extensively investigated, particularly in the context of Wavelength Division Multiplexing Passive Optical Networks (WDM PONs). In WDM PONs, which are filterless networks over a tree fiber topology, an arrayed waveguide grating (AWG) is typically adopted to multiplex/demultiplex different wavelength channels in a link between the Optical Line Termination (OLT) located in a central office and each Optical Network Unit (ONU). Typically, the AWG is built in a cyclic fashion, directing a certain wavelength in downstream to a certain ONU and another wavelength (e.g., in another wavelength band) upstream to the Optical Line Terminal (OLT) [27]. Although, WDM-PONs with carrier or wavelength reuse schemes have also been considered e.g. [31], [32], designing filterless metro networks that support bidirectional transmission requires to account for several specific aspects that are not present in WDM-PONs. For example, the topology is horseshoe and not tree, multiple nodes are traversed in pass-through mode, and a cascade of amplifiers has to be traversed.

Conclusively, the design of a filterless metro network exploiting bidirectional transmission over a single fiber is a branch of filterless networks that has not been studied in-depth yet.

3. A FILTERLESS BIDIRECTIONAL SINGLE-FIBER METRO

A traditional filterless node architecture using two unidirectional fibers is shown in Fig. 1(b). Signal add/drop is implemented by splitters and couplers while amplification of pass-through channels is performed by EDFAs, safely operating over unidirectional fibers. The filterless node architecture designed for bidirectional inter-node communication over a single fiber is shown in Fig. 2.

To support bidirectional inter-node communication over a single fiber, it is necessary to introduce optical circulators. These components are low-cost passive devices that typically provide less than 1 dB attenuation on the clockwise direction and more than 40 dB isolation on the counter-clockwise. Thanks to optical circulators, bidirectional communication can be implemented along the fiber interconnecting two adjacent nodes while unidirectional communication is implemented within the two branches of the node. This enables the EDFAs to properly operate and safely support add/drop onto the attached tributary interfaces.

The design of the filterless node architecture enabling inter-node counter-propagation has to consider three main constraints. The first constraint refers to the span and component losses (i.e., splitter/coupler and circulators) which have to be compensated through the proper setting of the EDFA amplifier gain. Indeed, the gain value has to be sufficiently high to compensate the losses, but below the threshold leading to lasering effects (i.e. light recirculation) in the potential loop between the two branches of the node. The second constraint refers to the overall optical reach of the horseshoe and in particular to the transmission impairments. Differently with respect to unidirectional transmissions, Rayleigh scattering becomes relevant. Indeed, both the optical signals and the ASE noise introduced by the amplifiers are reflected and propagated in the reverse direction together with the counter-propagating signal. The impact of these reflections is relevant due to the presence of optical amplification, experiencing a quadratic growth with the EDFA gain and the number of traversed nodes. The third aspect to consider refers to the spectrum assignment, which has to be implemented taking into account both accumulated impairments and target reach, possibly minimizing the impact of some effects such as scattering and crosstalk.

We assume a horseshoe metro network encompassing up to N links, interconnecting the Central Office with N metro-access nodes. Each node is designed to compensate for span length and component loss. As shown in the figure, each node includes two circulators to initiate and terminate the two branches. In addition, for each branch, one EDFA is introduced for loss compensation. One variable optical attenuator (VOA) is also included to guarantee adequate flexibility in optical power configuration. Finally, splitters/couplers are used for add/drop. Among the possible interconnection options of these components, the design presented in Fig. 2 is here considered since it enables large flexibility in compensating the attenuation of various link lengths, even links of 80 km (by just increasing the EDFA gain). Note that, in case of links of limited lengths, e.g. below 20-40 km depending on the receiver sensitivity, only one every two consecutive nodes may be equipped with EDFA. In this work we focus on the former scenario of Fig. 2 with EDFA at every node since it represents a worst case where scattering effects are more detrimental compared to the latter case where re-amplification is not performed at every node.

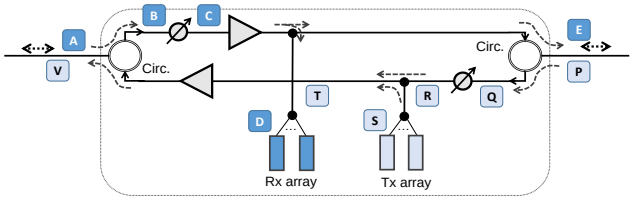

Fig. 2: Proposed filterless node for bidirectional single-fiber transmission

The design of the node architecture accounts for the following parameters: (1) $N = 10$ nodes in the considered horseshoe metro-access network; (2) link length between $L_{MIN} = 10$ km and $L_{MAX} = 50$ km, in line with typical metro range (larger distances could be also supported by the scheme); (3) splitting/coupling ratio of *1:2* in-line (3 dB loss) and at least *1:8* (12 dB loss) for add/drop (enabling interconnection of eight interfaces per node, even if larger values could be applied if necessary); (4) EDFA gain, in the case of L_{MAX}, of up to $G = 15$ dB (or larger); (5) Optical launch power at the exit of each node is designed to be $P_E = P_V = 0$ dBm (points *E* and *V* in Fig. 2). The optical power entering the node (points *A* and *P* in Fig. 2) depends on the link length: for the considered cases, it remains in the range between $-10\ dBm \le P_E = P_V \le -2\ dBm$. Circulators are assumed with typical values of *1dB* attenuation and *40 dB* isolation. The latter value, significantly higher than amplifier gain, guarantees that no light recirculation takes place within the node. The VOA in the upper *A–E* direction is introduced in case of link lengths lower than L_{MAX}, such that the optical power entering the EDFA is fixed at $P_C = -11\ dBm$. Given the above EDFA gain, the optical power exiting the node is, as anticipated, $P_E = 0$ dBm while at the RX interface is $P_D = -8\ dBm$ (largely within the typical sensitivity values). In the lower *P-V* direction, the VOA is configured, according to the link length, to fix the power $P_R = -11$ dBm. This way, assuming a TX interface power of $P_S = -2\ dBm$, all express and added channels are equalized at $P_T = -14\ dBm$, leading to $P_V = 0\ dBm$. Interfaces are assumed at 100 Gb/s with PM-QPSK modulation format. To summarize, node attenuation due to two circulators (1 dB loss each) and 3dB coupler/splitter is compensated, together with span loss by EDFA+VOA such that launch power is 0 dBm.

Given the above parameters and considering link lengths of 50 km of standard G.652 fiber, Fig. 3 presents the in-band crosstalk effect due to the Rayleigh scattering as a function of the traversed nodes, obtained by means of VPI simulation. Results show that the RX at the node *1* receives just a single scattering contribution, leading to less than -25 dB crosstalk due to reflected power. Instead, the signal generated at node *10* towards the central office is re-amplified at each of the *10* traversed nodes, leading to *10* scattering contributions that cumulate at the RX of node *10* to a crosstalk of around *-15.4dB*. Table I shows the overall performance of the considered single-fiber bidirectional filterless network after *N=10* traversed nodes, considering different link lengths. Considering ASE noise, results show that good OSNR performance is achieved, in the range between *26.4* and *27.6 dB*, with very limited sensitivity to link length. Results also show that in-band crosstalk is the dominating impairment, whose levels vary from *-22 dB* for *20 km* links to the *-15.4 dB* for *50 km* as indicated above.

Table I. Simulation results: expected OSNR and XTalk levels for different link lengths

Link Length [km]	*OSNR [dB] 0.1nm*	*Signal/Xtalk ratio [dB]*
20	27.6	-22
30	27.2	-19.6
40	26.7	-17.4
50	26.4	-15.4

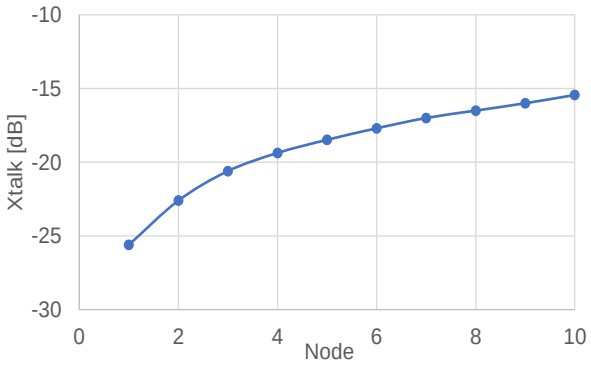

Fig. 3: In-band Crosstalk power as a function of the number of traversed nodes inducing Rayleigh scattering.

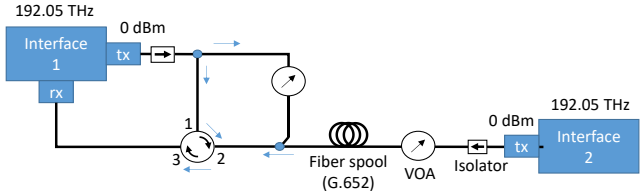

Fig. 4: Testbed setup

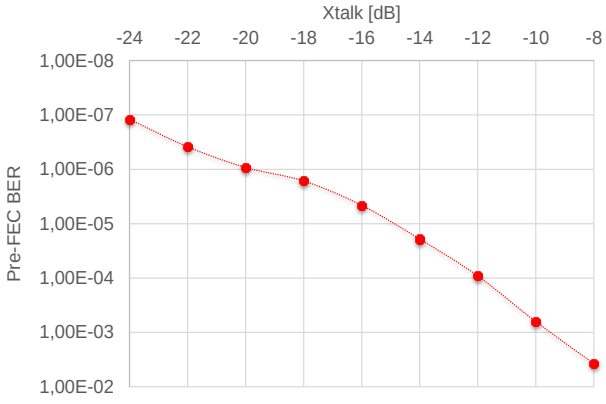

Fig. 5: Measured Pre-FEC BER at OSNR 27dB as a function of the in-band crosstalk

4. EXPERIMENTAL ASSESSMENT

In this section we present the experimental validation of a portion of the considered horseshoe metro network supporting bidirectional transmission. The testbed setup, shown in Fig. 4, emulates the transmission between the central office and the *i-th* network node. Commercial *100 Gb/s* PM-QPSK interfaces are considered. The considered link length is *25 km (G.652)*. To validate the scenario under different conditions, OSNR and crosstalk are varied to reproduce the simulation conditions. In particular, the in-band crosstalk is varied by introducing an additional counter-propagating and independent *100 Gb/s* PM-QPSK signal (interface 2 in Fig. 4) at the same central frequency (192.05 THz) and with configurable power level.

Fig. 5 shows the experimental measurements of the Pre-FEC BER as a function of the in-band crosstalk. Measurements are collected at *27 dB* OSNR (noise loading implemented by using an open input EDFA), thus reproducing the conditions assessed through simulations and related to a horseshoe of 10 links. Results show that, at the expected worst case conditions indicated by the simulations, i.e. at -15.4 dB signal-to-crosstalk ratio, the single-fiber bidirectional filterless network properly operates, experiencing a pre-FEC BER safely around 10^{-5}. Large margin is experienced since the system successfully operates until a crosstalk limit value of -8 dB (pre-FEC BER around 10^{-3}). Some margin of accuracy should be considered since all interferent power is added over a single span and not along an EDFA chain. Furthermore, different receivers, using different digital signal processing implementations, may experience different behavior. However, even considering some additional margin, the experienced pre-FEC BER remains largely above threshold. The measurements in Fig. 5 are performed assuming a nominal 50 GHz spectrum assignment perfectly aligned between the two counter-propagating directions.

In case the perfect alignment is deliberately not applied, a significant crosstalk reduction can be achieved. In particular, by applying a shift of 25 GHz between the two directions, the experienced crosstalk is reduced to the contributions due only to back-scattered ASE noise. Fig. 5 shows that, in case of extremely limited or no relevant in-band crosstalk, the system operates at extremely good performance, i.e. with pre-FEC BER above 10^{-6} after 10 links of 50 km.

5. PHYSICAL LAYER MODELLING OF A MULTI-CHANNEL SYSTEM

In the previous section, the scalability limitations due to Rayleight backscattering induced crosstalk, which is a single channel effect, were experimentally validated. In this section a method to estimate the physical layer performance and the scalability limitations due to multi-channel transmission is derived.

A. Systems under study

We study five systems with different operational parameters and data transportation rates from 100 to 400 Gb/s (Table II). C-band is split in two equal sub-bands, one for each propagation direction whilst the sum of channels from both directions is shown in the last column of Table II. The number of channels is a function of channel spacing, where, in the case of 100G line-rate, two variants are considered: a denser one with 37.5 GHz channel spacing and a coarser one with 50 GHz spacing. In addition, in the case of 400G channels, two different options are envisaged: the first assuming PM-16QAM channels and 75 GHz

channel spacing and a denser one which is compatible with the 50 GHz ITU-T grid, considering PM-64QAM channels. The parameters of Table II were selected in order to represent typical parameters of commercially available systems.

Table II. Details of the examined systems

	Modulation Format	*Symbol Rate (Gbaud)*	*Channel Spacing (GHz)*	*Data Rate (Gb/s)*	*Req. OSNIR (dB) (BER=10-3)*	*Max Num of Channels*
100G	PM-QPSK	32	37.5	100	9.8	116
	PM-QPSK	32	50	100	9.8	87
200G	PM-16QAM	32	37.5	200	16.55	116
400G	PM-16QAM	63	75	400	16.55	58
	PM-64QAM	42	50	400	22.5	87

B. Proposed Formalism

The dominant physical layer constraints due to the presence of optical amplifiers and the large number of channels are expected to be ASE noise and Four Wave Mixing (FWM). Making the assumption that FWM is statistically independent from ASE noise while considering it as an additive Gaussian noise source, we can calculate the Optical Signal to Noise plus Interference Ratio (OSNIR) as follows [33]:

$$OSNIR = \frac{P_{ch}}{P_{ASE} + P_{FWM}} \quad \textbf{(1)}$$

Then, we can directly estimate BER for various modulation formats [34]:

$$BER_{QPSK} = \frac{1}{2} erfc\left(\sqrt{\frac{OSNIR}{2}}\right),\ BER_{16QAM} = \frac{3}{8} erfc\left(\sqrt{\frac{OSNIR}{10}}\right) \quad \textbf{(2)}$$
$$BER_{64QAM} = \frac{7}{24} erfc\left(\sqrt{\frac{OSNIR}{42}}\right)$$

Using (2) and setting a target BER of 10^{-3}, the required OSNIR is about 9.8, 16.55 and 22.5 dB for PM-QPSK, PM-16QAM and PM-64QAM respectively. As expected, higher modulation formats require a greater OSNIR value in order to attain the same BER. The power of ASE noise can be calculated as $P_{ASE} = N_s hf\left(NF \cdot G - 1\right) B_o$ where *NF* is the EDFA noise figure which in our case equals to 6 dB, *G* represents the EDFA Gain which compensates exactly the fiber loss plus an extra of 5 dB (3 dB for the coupling loss and 2 dB for the circulator loss). Finally, N_s represents the number of Metro Nodes a channel is traversing and B_o the optical bandwidth.

Regarding the calculation of FWM, expressions such as the GN model [35] or [36] cannot be employed since they assume co-propagating channels. In this work, where bi-directional transmission is considered, some modifications are required. Herein, we are based on the expression of [33], which will be modified to account for counter-propagating channels. This formula is selected because it is closed-form, thus allowing to perform fast OSNIR optimizations, whilst it provides very good accuracy within the metro domain, where the inter-node distances are typically smaller than 30 km. Other solutions, such as the closed-form GN-model [35] or [36], are leading to erroneous estimations when the inter-node distance is smaller than 35 km, due to their employed approximations.

An important difference between the quantities OSNR and OSNIR is the optical bandwidth that needs to be taken into account in the two respective cases. In the former case, B_o has a typical value of 0.1 nm. During the Non-Return to Zero (NRZ) era, the speed at that time was mainly at 10 Gb/s, meaning that the largest fraction of the optical power was within an optical bandwidth of 0.1 nm. Moreover, as the ASE noise is treated as a white noise at system level, it made no difference the bandwidth over which this signal-to-noise ratio is estimated, provided it was the same for signal and noise. Thus, 0.1 nm was used as a reference. In this work, the systems under study are based on Nyquist-WDM or coherent optical orthogonal frequency division multiplexing where the optical power is equally distributed between the frequencies in a channel. Thus, when OSNIR is used as a merit function, to account for nonlinearities, the optical bandwidth B_o should be set to a value that spans the entire channel because of two reasons: a) the total power of the channel has to be calculated and b) new frequencies are generated within the channel bandwidth due to FWM. Therefore, B_o for any system, equals to the equivalent symbol rate shown in Table II. Further, when rectangular spectra channels are employed, the number of generated frequencies due to FWM is significantly larger when compared with NRZ channels, making FWM dominate over SPM and XPM. Next, the power of FWM crosstalk can be disjoined into the following components: a) $P_{FWM,intra}$, which accounts for the interactions between the frequencies within the observed channel only, b) $P_{FWM,inter,co\text{-}prop}$, which accounts for the interactions between the observed channel and the co-propagating channels and c) $P_{FWM,inter,counter\text{-}prop}$ which accounts for the interactions between the observed channel and the counter-propagating channels. The expressions (a) and (b) are directly derived from [33], after performing some simple algebra, as follows:

$$P_{FWM,intra} = \frac{32}{27}\frac{\gamma^2 {L_{eff}}^2 {P_{ch}}^3 {N_s}^2 c}{\lambda^2 B^2 D\sqrt{z_1}}\left(1+\frac{4e^{-aL}}{\left(1-e^{-aL}\right)^2}\right) asinh\left(\frac{\pi\lambda^2 DB^2}{8c}\sqrt{z_2}\right) \quad \textbf{(3)}$$
$$-\frac{32}{27}\frac{\gamma^2 {L_{eff}}^2 {P_{ch}}^3 {N_s}^2 c}{\lambda^2 B^2 D\sqrt{z_1+12L^2}}\frac{4e^{-aL}}{\left(1-e^{-aL}\right)^2} asinh\left(\frac{\pi\lambda^2 DB^2}{8c}\sqrt{z_2+12L^2}\right)$$

$$P_{FWM,inter,co\text{-}prop} = \sum_{n=-\frac{N_{ch}-1}{2},n\neq 0}^{\frac{N_{ch}-1}{2}} P_n^2\left(1-\frac{5}{6}\Phi_n\right)\left|Log\left(\frac{n+1/2}{n-1/2}\right)\right|\times \quad \textbf{(4)}$$
$$\frac{32}{27}\frac{\gamma^2 {L_{eff}}^2 P_{ch} {N_s}^2 c}{\lambda^2 B^2 D}\left(\frac{1}{\sqrt{z_1}}\left(1+\frac{4e^{-aL}}{\left(1-e^{-aL}\right)^2}\right)-\frac{1}{\sqrt{z_1+12L^2}}\frac{4e^{-aL}}{\left(1-e^{-aL}\right)^2}\right)$$

where $z_1 = \left(\frac{2}{a}\right)^2 + 2L^2\left(N_s^2-1\right)/\left(\sum_{k=x_1}^{x_2}\frac{1}{1+\left(2k\pi/(aL)\right)^2}\right)^2$,

$x_1 = -\frac{\lambda^2 B^2 DLN_{ch}^2}{16c}$ $x_2 = \frac{\lambda^2 B^2 DLN_{ch}^2}{2c}$ and $z_2 = \left(\frac{2}{a}\right)^2 + 2L^2\left(N_s^2-1\right)$

with x_1 and x_2 rounded to the nearest integer less than or equal to their values. The index n includes all co-propagating channels of the link and takes values within the range $-\left(N_{ch}-1\right)/2 \le n \le \left(N_{ch}-1\right)/2$. P_{ch} and P_n denote the power of the observed and the n^{th} interfering channel, respectively. L is the inter-node distance, B is the optical bandwidth and Φ_n is a modulation format depended parameter which takes the value

of 1, 17/25 and 13/21 when QPSK, 16QAM and 64QAM are employed, respectively.

Regarding the case (c), [33] cannot be directly applied, since the power evolution direction of the examined channel is different compared to the power evolution direction of the interfering channels. This is shown in Fig. 6 where f_1 and f_2 correspond to the central frequencies of the observed and the interfering channel, respectively. As it is evident from Fig. 6, in the counter-propagating case, there are two areas where the FWM is mainly generated: within the effective length of the observed channel, and within the effective length of the counter-propagating channel. The former is designated as $L_{eff,mod,1}$ whilst the latter as $L_{eff,mod,2}$. The effective length is considered as the equivalent length of a lossless fiber where the nonlinear interference occurs. In case (c), the two "*modified*" effective lengths have to be calculated in order to account for the power evolution of both channels as follows

$$L_{eff,\mathrm{mod},1} = -\int_{L_{eff,f1}}^{0} e^{-a_2(L-z)}dz = \frac{e^{-a_2 L}}{a_2}\left(e^{\frac{a_2 - a_2 e^{-a_1 L}}{a_1}} - 1\right)$$
$$L_{eff,\mathrm{mod},2} = \int_{L-L_{eff,f2}}^{L} e^{-a_1 z}dz = \frac{e^{-a_1 L}}{a_1}\left(e^{\frac{a_1 - a_1 e^{-a_2 L}}{a_2}} - 1\right) \quad (5)$$

where a_1 and a_2 represent the fiber attenuation parameters of the two propagation directions. In this work we assume that $a_1 = a_2 = a = 0.2$ dB/km. As a consequence, $L_{eff,mod,1} = L_{eff,mod,2}$ and are equal to 6.11 and 7.14 km when L = 10 and 20 km, respectively.

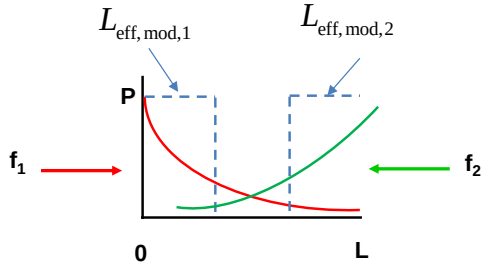

Fig. 6. Power evolution of two counter-propagating channels.

After Eq.(5), we have that

$$P_{FWM,inter,counter-prop,i} = \sum_{n=-\frac{N_{ch}-1}{2},n\neq 0}^{\frac{N_{ch}-1}{2}} P_n^2\left(1-\frac{5}{6}\Phi_n\right)\left|Log\left(\frac{n+1/2}{n-1/2}\right)\right| \times \frac{32}{27}\frac{\gamma^2 L_{eff,mod,i}^{\ 2} P_{ch} N_s^{\ 2} c}{\lambda^2 B^2 D}\left(\frac{1}{\sqrt{z_1}}\left(1+\frac{4e^{-aL}}{\left(1-e^{-aL}\right)^2}\right)-\frac{1}{\sqrt{z_1+12L^2}}\frac{4e^{-aL}}{\left(1-e^{-aL}\right)^2}\right) \quad (6)$$

where i takes the values of 1 and 2 in order to include both areas of Fig. 6 whilst n includes the indices of all counter-propagating channels. Table III summarizes the parameters considered in our physical layer studies.

Table III. Details of system parameters considered in the physical layer studies

Parameter	*Symbol*	*Value*
fiber attenuation	a	0.2 (dB/km)
local dispersion	D	17 (ps/nm/km)
nonlinear coefficient	γ	1.3 (1/W/km)
noise figure	NF	6 (dB)
amplifier gain	G	a·L + 5 (dB)
inter node distance	L	10, 20 (km)
central wavelength	λ	1550 (nm)
modulation format FWM dependence	Φ	1 for QPSK, 17/25 for 16QAM, 13/21 for 64QAM

C. Impact of Operational Parameters

As shown in Table II, the examined systems have different operational parameters. This will directly affect the strength of physical layers effects which will in turn impact the overall OSNIR performance. Accordingly, FWM is a function of the modulation format, through the parameter Φ_n, which results to a higher P_{FWM} when the modulation format increases. Next, the optical bandwidth affects both ASE noise and FWM: the ASE noise is proportional whilst the FWM is inversely proportional to B. The latter can be attributed to the fact that the power level of each interfering frequency component is smaller. Next, the higher number of channels leads to a larger number of interfering frequencies and in turn to stronger inter-channel nonlinearity. As a result, a variation of both linear and nonlinear effects is expected between the five examined systems. We also consider that all channels of a system have equal power, as the amplification gain is considered the same for all channels. This assumption is reasonable in order to perform meaningful quantitative comparisons across all examined systems, however, the proposed formalism allows for unequal channel power and modulation format by properly setting the parameters P_n and Φ_n, in Eq.(4) and (6).

6. PERFORMANCE ASSESSMENT

A. Assessing optimum power

In order to maximize the node cascadeability we need to calculate the optimum power P_{opt} which maximizes OSNIR. Accordingly, when $P_{ch} < P_{opt}$ the system is ASE limited and when $P_{ch} > P_{opt}$ the system is nonlinearity limited. The optimum power is expected to differ between each system based on the operational parameters. This is obvious in Fig. 7, which shows the OSNIR for various channel power levels for all five examined systems. The attainable P_{opt} value for each system is also shown in Table IV. The OSNIR is estimated in the central channel of the upper sub-band. When comparing the cases of 100G with 200G it is evident that the higher modulation format leads to significantly stronger FWM. Further, it is evident that the 400G channels are more vulnerable to ASE noise compared with 100 and 200G channels due to the higher optical bandwidth. This in turn, will lead to an increase of the P_{opt} in the case of 400G channels. Next, the case of 400G with 64QAM attains the lowest maximum OSNIR due to both a) the higher ASE noise due to the larger optical bandwidth and b) the stronger FWM crosstalk due to the higher modulation format. Finally, the case when inter-node distance equals to 20 km performs almost 2 dB worse than

the case of 10 km due to the higher amplification gain needed to compensate the additional fiber loss.

Table IV. Optimal channel power for different systems

	L = 10 km		*L = 20 km*	
	P_{opt} *(dBm)*	*OSNIR (dB)*	P_{opt} *(dBm)*	*OSNIR (dB)*
100G-PM-QPSK (37.5 GHz)	-3	25.9	-2	24.1
100G-PM-QPSK (37.5 GHz)	-3	26.0	-2	24.2
200G-PM-16QAM (37.5 GHz)	-3	25.2	-3	23.6
400G-PM-16QAM (75 GHz)	-1	25.0	0	23.4
400G-PM-64QAM (50 GHz)	-2	25.0	-2	23.3

Based on the above remarks we can draw an important conclusion which is that the optimum power should be system tailored, instead of simply selecting a single "global" optimum power value for all cases, in order to ensure a maximization on the overall performance.

B. Node cascadeability

The OSNIR evolution versus the number of Metro Nodes is shown in Fig. 8. In order to calculate the node cascadeability, the optimum power of each system is selected. As it is evident, when QPSK or 16QAM channels are deployed, the attainable OSNIR clears the threshold for a BER < 10^{-3}, even after 20 Nodes, remaining always above 16.55 dB. In contrast, when 64QAM channels are transmitted, the signal can traverse up to 18 and 12 Nodes when the inter-node distance is set to 10 and 20 km, respectively, for a BER < 10^{-3} which corresponds to an OSNIR threshold of 22.5 dB.

Results also show that 100G channels outperform 200 and 400G channels in all cases. This is attributed mainly to the lower modulation format (QPSK), which compared to 16 and 64QAM leads to lower FWM crosstalk.

Finally, a quantitative comparison between all five systems is performed considering a channel power equal to 0 dBm for all cases (Fig. 9). This power stresses all systems, except 400G with 16QAM, to work in nonlinear regime, as this power is larger than Popt. This decision can be made under the assumption that the system will not be fully loaded with channels, where the impact of FWM is expected to be lower. As it can be deduced from Fig. 9, the case of 400G employing 16QAM channels, attains the highest OSNIR, since it works close to its optimum power. In contrast, the case of 200G channels attains the worst OSNIR performance since it works in deeply nonlinear regime, where FWM dominates. The cost of this shift from Popt (Fig. 8) to 0 dBm (Fig. 9) depends on the system characteristics and varies between 0 and 3.3 dB in terms of OSNIR. Finally, the higher channel spacing of 50 GHz, compared to 37.5 GHz spacing, in 100G channels, provides a marginal OSNIR improvement of about 0.3 dB but at the cost of a decreased number of channels.

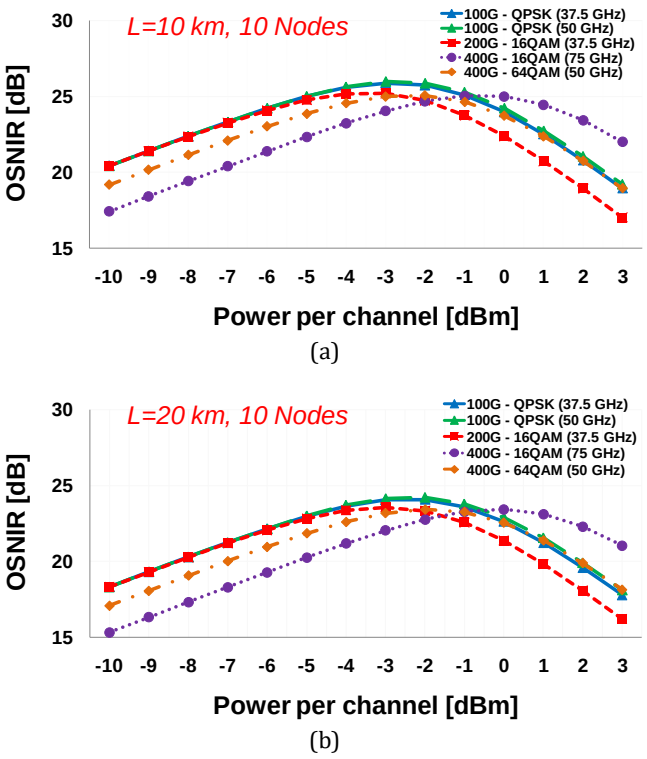

(a)

(b)

Fig. 7. OSNIR as a function of P_{ch} for a) 10 km and b) 20 km inter-node distance after 10 Nodes.

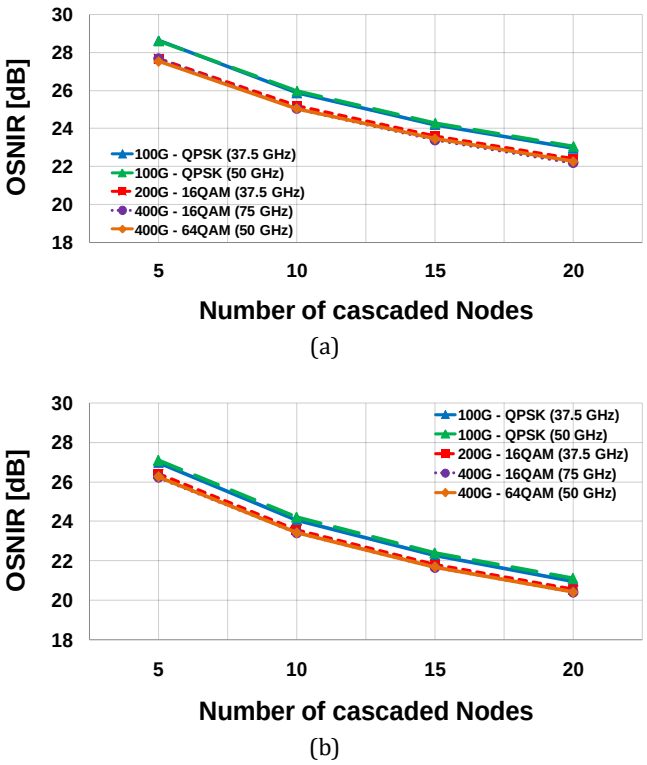

(a)

(b)

Fig. 8. OSNIR as a function of the number of Nodes for a) 10 km and b) 20 km when the optimum power is set in each case.

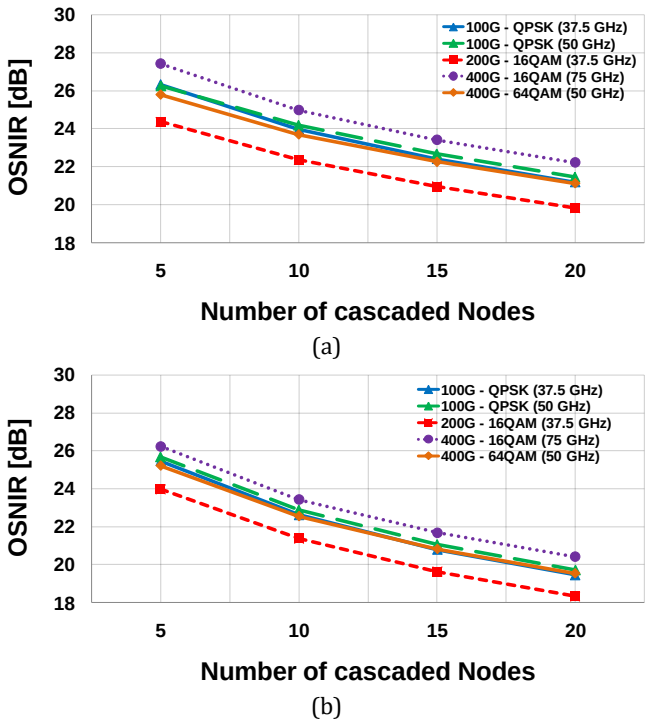

Fig. 9. OSNIR as a function of the number of Nodes for a) 10 km and b) 20 km when a P_{ch} = 0 dBm is set in all cases.

7. CONCLUSIONS

In this paper, we propose, study and validate a filterless Metro network exploiting bidirectional transmission over a single fiber in a horseshoe topology. We elaborate the mode of operation and we detail the corresponding node architecture. The performance of the system is estimated via simulations taking into account single channel effects like OSNR and Crosstalk after 10 spans of typical Metro lengths (i.e. between 10 and 50 km). The results are benchmarked against those from the corresponding experimental measurements with a 100 Gb/s commercial coherent system, showing to be in a very good agreement. Moreover, an operational margin of 7 dB is found to be adequate when two identical channels are launched in the two opposite directions of the Metro link. By applying a 25GHz misalignment between the two directions, we measured an extremely good performance (pre-FEC BER above 10^{-6} after 10 links of 50 km). Then, we present a methodology to estimate the physical layer performance and the scalability of a multi-channel bidirectional system while deriving system parameters like the optimal launch power. The result from these physical layer studies reveal that QPSK and 16QAM channels can traverse more than 20 Nodes with sufficient BER performance whilst a system with 64QAM channels can cascade more than 12 Nodes. Finally, it was shown that operating the system far from the optimum power can cause an OSNIR degradation of more than 3 dB. The sufficient attainable performance on both single and multi-channel transmission confirms that a horseshoe filterless network exploiting bidirectional transmission over a single fiber represents an extremely attractive metro network solution. This is expected to become even more attractive with the widespread availability of low-cost coherent pluggable modules. As a future step, the simulation model and results in the case of multiple channels can be validated experimentally.

Funding Information. This work has received funding from the ECSEL Joint Undertaking (JU) BRAINE Project under grant agreement No 876967. The JU receives support from the European Union's H2020 research and innovation programme and from Italy Ministry of Education, University and Research (MIUR).
Acknowledgment. We thank Pantea Nadimi Goki for the contribution to the experimental assessment.

References

1. N. Le Sauze; A. Dupas; E. Dotaro; L. Ciavaglia; M. Nizam; A. Ge; L. Dembeck "A novel, low cost optical packet metropolitan ring architecture," in Proc. 27th European Conf. Optical Communication ECOC'01, vol. 6, Amsterdam, Netherlands, Sept.–Oct. 2001, pp. 66–67.
2. http://monarchna.com/OADMLC-NoWavelengthReuse-Rings-2000.pdf
3. L.Dittman, C. Develder, D. Chiaroni, F. Neri, F. Callegati, W. Koerber, A. Stavdas, M. Renaud, A. Rafel, J. Pareta, N. Leligou, Lars Dembeck, B. Mortensen, M. Pickavet, N. Le Sauze, M. Mahony, Bela Berde, G. Eilenberger, "The European IST Project DAVID: a Viable Approach towards Optical Packet Switching". IEEE Journal of Selected Areas on Communications, Vol. 21 (7), pp.1026-1040, 2003.
4. S. Sygletos, C. Skoufis, C. Matrakidis, A. Stavdas, N. LeSauze and D. Chiaroni, "Physical Layer Performance Benchmarking of Two Metropolitan Area Network Configurations." Optical Switching and Networking, Volume 2, Issue 1, pp 19-33, May 2005
5. C. Develder, A. Stavdas, A. Bianco, D. Careglio, R. Van Caenegem, S. Sygletos, F. Neri, J. Solé-Pareta, M. Pickavet, "Benchmarking and viability assessment of Optical Packet Switching for Metro Networks", IEEE Journal of Lightwave Technology, Special Issue on Metro and Access Networks, Vol.22, no.11, pp. 2435-2451, 2004
6. C.Tremblay, F. Gagnon, B. Chatelain, E. Bernier, and M. Belanger, "Filterless optical networks: a unique and novel passive WAN network solution," in 12th OptoElectronic and Communications Conference (OECC)/ 16th International Conference on Integrated Optics and Optical Fiber Communication (OECC/IOOC'07), July 2007, pp. 12P–7.
7. E. Archambault, N. Alloune, M. Furdek, Z. Xu, C. Tremblay, A. Muhammad, J. Chen, L. Wosinska, P. Littlewood, and M. P. Belanger, "Routing and spectrum assignment in elastic filterless optical networks," IEEE/ACM Transactions on Networking, vol. 24, no. 6, pp. 3578–3592, December 2016.
8. Z. Xu, E. Archambault, C. Tremblay, J. Chen, L. Wosinska, M. P. Belanger, and P. Littlewood, "1+1 dedicated optical-layer protection strategy for filterless optical networks," IEEE communications letters, vol. 18, no. 1, pp. 98–101, 2014.
9. B. Jaumard, Y. Wang, and N. Huin, "Optimal design of filterless optical networks," in 2018 20th International Conference on Transparent Optical Networks (ICTON), July 2018, pp. 1–5.
10. B. Zaluski, B. Rajtar, H. Habjanic, M. Baranek, N. Slibar, R. Petracic, and T. Sukser, "Terastream implementation of all ip new architecture," in 2013 36th International Convention on Information and Communication Technology, Electronics and Microelectronics (MIPRO), May 2013, pp. 437–440.
11. O. Ayoub, S. Shehata, F. Musumeci, and M. Tornatore, "Filterless and semi-filterless solutions in a metro-haul network architecture," in 2018 20th International Conference on Transparent Optical Networks (ICTON), July 2018, pp. 1–4.
12. B. Shariati, M. Ruiz, A. Sgambelluri, F. Cugini, and L. Velasco, "Real-time spectrum surveillance in filterless optical networks," in 2018 Optical Fiber Communications Conference and Exposition (OFC), March 2018, pp. 1–3.

13. F. Cugini, C. Porzi, N. Sambo, A. Bogoni, and P. Castoldi, “Receiver architecture with filter for power-efficient drop waste networks,” in 2016 Optical Fiber Communications Conference and Exhibition (OFC), March 2016, pp. 1–3.
14. M. Furdek, A. Muhammad, G. Zervas, C. Tremblay, and L. Wosinska, “Performance evaluation of programmable filterless networks implemented by optical white boxes,” in 2016 18th International Conference on Transparent Optical Networks (ICTON), July 2016
15. C. Tremblay, P. Littlewood, M. P. B´elanger, L. Wosinska, and J. Chen, “Agile filterless optical networking,” in 2017 International Conference on Optical Network Design and Modeling (ONDM), May 2017, pp. 1–4.
16. C.Tremblay, “Agile Optical Networking: Beyond Filtered Solutions”, OFC, 2018
17. Karandin et al “A Techno-Economic Comparison of Filterless and Wavelength-Switched Optical Metro Networks”, ICTON 2020
18. Savoie et al, “Physical layer validation of Filterless optical networks", ECOC 2010
19. Emmerich et al. “Capacity Limits of C+L Metro Transport Networks Exploiting Dual-Band Node Architectures” OFC 2020
20. Dochhan et al. "Flexible metro network architecture based on wavelength blockers and coherent transmission" ECOC 2019
21. D. Uzunidis, E. Kosmatos, C. Matrakidis, A. Stavdas, and A. Lord, “DuFiNet: Architectural considerations and physical layer studies of an agile and cost-effective metropolitan area network,” Journal of Lightwave Technology, vol. 37, no. 3, pp. 808–814, Feb 2019.
22. F. Paolucci, R. Emmerich, F. Fresi, I. Sackey, L. Poti, C. Schubert, J. Fischer, and F. Cugini, “Filterless optical WDM metro networks exploiting C+L band,” in 2018 European Conference on Optical Communications (ECOC 2018), Sept 2018.
23. F. Paolucci, R. Emmerich, A. Eira, N. Costa, J. Pedro, P. W. Berenguer, C. Schubert, J. K. Fischer, F. Fresi, A. Sgambelluri, and F. Cugini, “Disaggregated edge-enabled C+L-band filterless metro networks”, IEEE/OSA Journal of Optical Communications and Networking, vol. 12, no. 3, pp. 2–12, March 2020.
24. F. Paolucci, A. Sgambelluri, R. Emmerich, A. Giorgetti, P. Castoldi, C. Schubert, J. Fischer, and F. Cugini, “OpenConfig control of 100G/400G filterless metro networks with configurable modulation format and FEC,” in Optical Fiber Communication Conference (OFC), 2019.
25. E. Kosmatos, D. Uzunidis, C. Matrakidis, A. Stavdas, S. Horlitz, Th. Pfeiffer, A.Lord; “Building a Truly Dynamic Filterless Metro Network by Reusing a Commercial PON's Data-Plane and a Novel SDN-Enabled Control-Plane”, OSA/IEEE Journal of Lightwave Technology, Vol.37, issue 24, pp. 6033 - 6039, 2019
26. F Cugini, A Sgambelluri, PN Goki, F Paolucci, M Presi, “Single-Fiber Bidirectional Filterless Metro Network”, International Conference on Optical Network Design and Modeling (ONDM), 2020
27. E. Kosmatos, D. Uzunidis, C. Matrakidis, A. Stavdas, S. Horlitz, Th. Pfeiffer, A.Lord; “Building a Truly Dynamic Filterless Metro Network by Reusing a Commercial PON's Data-Plane and a Novel SDN-Enabled Control-Plane”, OSA/IEEE Journal of Lightwave Technology, Vol.37, issue 24, pp. 6033 - 6039, 2019
28. A. Stavdas, T. Orphanoudakis, A. Lord, H.C. Lelligou, K. Kanonakis, C. Matrakidis, A. Drakos and J.D. Angelopoulos: “Dynamic CANON: A scalable inter-cluster multi-domain core network”, IEEE Communications Magazine, Vol.46 (6), pp. 138-144, June 2008
29. T. Orphanoudakis, A. Drakos, H-C Leligou, A.Stavdas, A. Boucouvalas, “Dynamic Resource Allocation with Service Guarantees over Large Scale Optical Networks”, IEEE Communication Letters, Volume 13, Issue 11, pp. 859-861, 2009.
30. A. Drakos, C. Matrakidis, T. Orphanoudakis, A. Stavdas: “A Node Clustering Algorithm for the CANON Architecture”, IEEE Communications Letters, Volume:17, Issue: 4, pp. 785 – 788, 2013
31. M. Presi, M. Rannello, M. Artiglia, I. Tomkos, I. Cano, J. Prat, and E. Ciaramella, “Hitless wavelength assignment in filterless optical access networks,” in 2016 18th International Conference on Transparent Optical Networks (ICTON), July 2016.
32. J. A. Lazaro, C. Arellano, V. Polo, and J. Prat, “Rayleigh scattering reduction by means of optical frequency dithering in passive optical networks with remotely seeded onus,” IEEE Photonics Technology Letters, vol. 19, no. 2, pp. 64–66, Jan 2007.
33. D. Uzunidis, C. Matrakidis, and A. Stavdas. "Closed-form FWM expressions accounting for the impact of modulation format." Optics Communications, vol. 440, pp.132-138, 2019
34. D. Uzunidis, C. Matrakidis, and A. Stavdas. "Optimizing power, capacity, transmission reach and amplifier placement in coherent optical systems using a physical layer model." In Proc. of the 20th Pan-Hel. Conf. on Inform., 2016.
35. P. Poggiolini, G. Bosco, A. Carena, V. Curri, Y. Jiang and F. Forghieri, "The GN-Model of Fiber Non-Linear Propagation and its Applications," in Journal of Lightwave Technology, vol. 32, no. 4, pp. 694-721, 2014
36. D. Uzunidis, C. Matrakidis and A. Stavdas, "Analytical FWM Expressions for Coherent Optical Transmission Systems," in Journal of Lightwave Technology, vol. 35, no. 13, pp. 2734-2740, 2017